Remote Sensing of Atmospheric Water Vapor and Liquid Water with the Nimbus 5 Microwave Spectrometer

D. H. STAELIN, K. F. KUNZI,[1] R. L. PETTYJOHN, R. K. L. POON[2] AND R. W. WILCOX[3]

Research Laboratory of Electronics, Massachusetts Institute of Technology, Cambridge, Mass. 02139

J. W. WATERS

Jet Propulsion Laboratory, California Institute of Technology, Pasadena 91103

(Manuscript received 26 January 1976, in revised form 6 October 1976)

ABSTRACT

The passive microwave spectrometer on the Nimbus 5 satellite has two channels that measure atmospheric water vapor and liquid water abundances over ocean. Observed water vapor abundances range up to 6 g cm^{-2} and differ from nearby radiosondes by ~0.4 g cm^{-2}. Average liquid water abundances over a 300 km observation zone range from −0.01 to 0.2 g cm^{-2}, and have an rms error estimated to be ~0.01 g cm^{-2} for most circumstances. These quantitative measurements can be used to construct global maps or to accumulate global statistics.

1. Introduction

Since 11 December 1972 the Nimbus 5 (Nimbus E) Satellite Microwave Spectrometer (NEMS) has been measuring 1) the atmospheric temperature profile 0–20 km, 2) the atmospheric water vapor and liquid water abundances over open ocean, and 3) geophysical parameters such as snow and ice distribution and type. Preliminary NEMS results were reported by Staelin *et al.* (1973) and observations made with NEMS from aircraft were discussed by Rosenkranz *et al.* (1972). The ability of NEMS to determine atmospheric temperature profiles and the influence of clouds upon those determinations have been discussed by Waters *et al.* (1975) and Staelin *et al.* (1975), respectively. Radiometric methods for measuring atmospheric water from space have also been discussed, together with samples of NEMS data, by Grody (1976).

One of the unique capabilities of passive microwave sensors in space is the ability to measure atmospheric water vapor and liquid water over ocean, even in the presence of most types of cloud. NEMS incorporates channels at 22.235 and 31.4 GHz for evaluation of this capability. The following data suggest that both water vapor and liquid water can be determined over ocean with meteorologically significant accuracies.

The use of microwave spectroscopy for atmospheric sensing evolved largely from radio astronomy techniques developed for probing the atmospheres of other planets and interstellar gases. Barrett and Chung (1962) first noted that the atmospheric water vapor profile could be determined from observations of the 22.235 GHz water vapor resonance, and such observations were later performed by Staelin (1966) who further noted that the water vapor and liquid water abundances in the atmosphere could be determined separately by virtue of their different spectral characteristics. Toong and Staelin (1970), using ground-based observations, subsequently demonstrated this ability to distinguish water vapor and liquid water.

The first water vapor microwave spectrometer in space was a two-channel radiometer on the Mariner-2 Venus probe (Barath *et al.*, 1964) which placed an upper limit on water vapor in the atmosphere of Venus and indicated that the planetary surface was near 600 K. Cosmos-243 (Basharinov *et al.*, 1969) and Cosmos-384 (Akvilonova *et al.*, 1973) orbited the earth and yielded data at frequencies near 3.5, 8.8, 22.235, and 37 GHz for approximately two weeks in September 1968 and two days in December 1970, respectively. These experiments permitted estimates of the integrated abundances of both water vapor and liquid water (g cm^{-2}) over ocean. The NEMS and Cosmos experiments differ in that the Cosmos instruments had 4 surface channels and somewhat greater angular resolution whereas NEMS data are more precise and exceed 2.4 continuous years.

The NEMS antennas observe nadir continuously at 22.235, 31.4, 53.65, 54.9 and 58.86 GHz with half-power antenna beam-widths of 10°. The instantaneous ground resolution is ~190 km, which is then smeared approx-

[1] Present affiliation: University of Bern, Bern, Switzerland.
[2] Present affiliation: Chinese University of Hong Kong, Shatin, Hong Kong.
[3] Present affiliation: Control Data Corporation, Minneapolis, Minn. 55440.

imately 100 km along the flight path by the 16 s integration during data processing. The instrument was fabricated at the Jet Propulsion Laboratory of the California Institute of Technology. The satellite orbit is sun-synchronous at an inclination of 100° and an altitude of 1096 km. Equator crossings occur near local noon and midnight.

The discussion of NEMS atmospheric water measurements begins here with a review of basic principles and a discussion of the accuracy of NEMS determinations of water vapor and atmospheric liquid water abundances. Observations of specific storms and fronts are then presented, followed by observations of water vapor and liquid water on a global scale. The concluding discussion surveys the NEMS results and some future opportunities.

2. Principles of atmospheric water determination

The 22.235 GHz channel is centered on the water vapor resonance arising from transitions between the rotational states 5_{23} and 6_{16}, and the 31.4 GHz channel lies in the window between this resonance and the broad 60 GHz band of oxygen. Even at the center of the 22.235 GHz resonance the atmosphere is quite transparent, typically absorbing less than 20% of the radiation propagating through it to space; the window absorption is typically half this value. Only in cumulonimbus or similar heavy clouds does the absorption exceed 70%, for water vapor and liquid water are the dominant absorbers at these two frequencies.

At microwave frequencies the terrestrial surface and troposphere are in local thermodynamic equilibrium and radiate with intensity directly proportional to the product of their temperature and emissivity. The microwave emissivity of land surfaces is typically near 0.8–1.0, and thus their brightness temperatures range from 0.8 to 1.0 times the land surface temperature. This land brightness is nearly the same temperature as the atmospheric water, which therefore appears strongly neither in emission nor in absorption. For this reason no determinations of atmospheric water content are made over land by NEMS. The ocean, however, has an emissivity near 0.45 at these wavelengths and thus, in the absence of any atmosphere, would have a microwave brightness temperature of ~130 K, much below the temperature of atmospheric water. Therefore the atmospheric water vapor and liquid water appear warm against this cool background.

Calculated water vapor and liquid water emission spectra over ocean appear in Fig. 1. The four theoretical spectra shown there correspond to 1) no atmosphere; 2) the 1962 U. S. Standard Atmosphere, plus a nominal winter water vapor distribution having 0.88 g cm^{-2} distributed exponentially as 4 $e^{-H/2.2}$ [g m^{-3}], where H is altitude in km; 3) the same plus a moderately dense low stratus cloud located at altitudes of 150–650 m with 0.25 g m^{-3} liquid water, equivalent to 0.0125 g cm^{-2}; and 4) the same standard atmosphere plus a nominal summer $10e^{-H/2.2}$ [g m^{-3}] water vapor distribution, equivalent to 2.2 g cm^{-2}.

The figure illustrates that the water vapor resonance differs markedly in form from the non-resonant emission by clouds, and thus the two NEMS measurements at 22.235 and 31.4 GHz permit the separate determination of these two components. Raining clouds have spectra similar to nonraining clouds but the spectra partly depend on the drop-size distribution. A typical rain of 2.5 mm h^{-1} might add nonresonant emission about 4 times the increment indicated for the stratus cloud (Goldstein, 1951). The water vapor absorption coeffi-

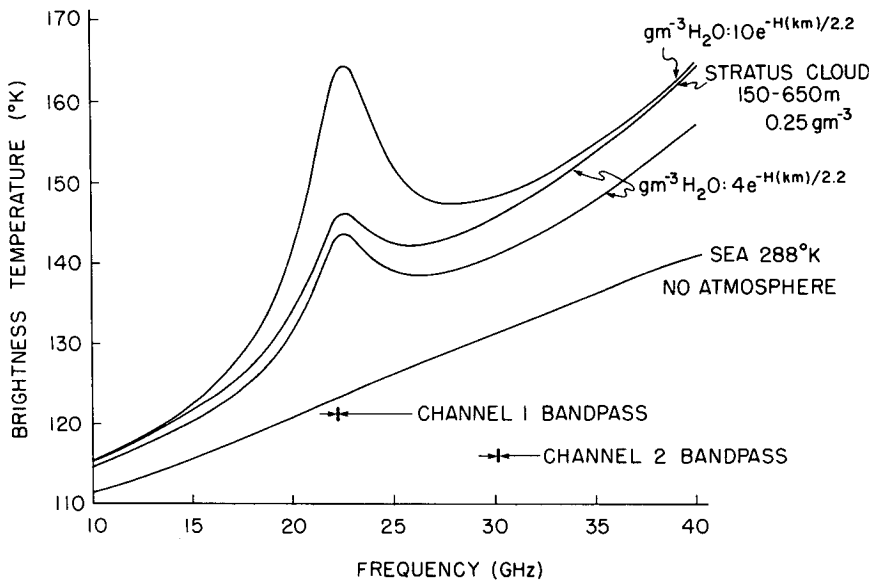

FIG. 1. Theoretical microwave brightness temperature spectra computed for a nadir-viewing satellite over ocean at 288 K.

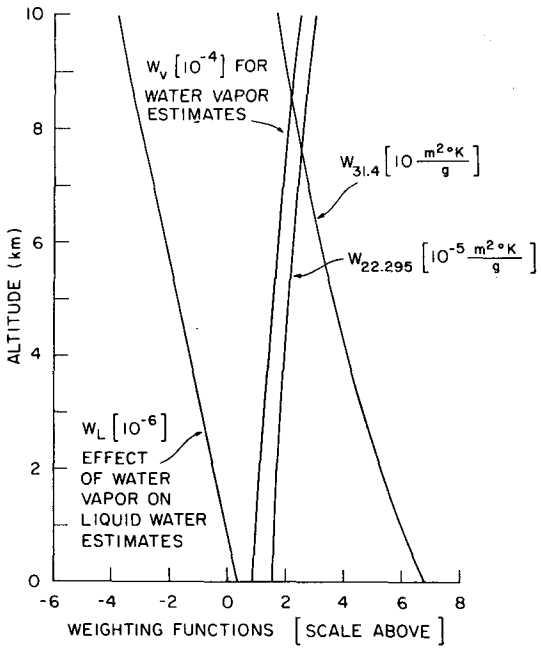

FIG. 2. Weighting functions for the effect of water vapor profiles on 31.4 GHz brightness temperature ($W_{31.4}$), 22.295 GHz brightness temperature ($W_{22.295}$), inferred water vapor abundance (W_v), and inferred liquid water abundance (W_L). The appropriate units for the horizontal scale are indicated in square brackets for each parameter.

cient used in the analysis is approximately that given by Barrett and Chung (1962).

The observed microwave emission spectra of liquid and vaporous water also depend upon other parameters such as the atmospheric temperature profile, the altitude distribution of the water, and the elevation and electromagnetic properties of the terrestrial surface. Variations and uncertainties in these parameters dominate NEMS retrieval accuracies. The uncertainties in the theoretical expressions for atmospheric transmittances are less important, as are the contributions of the wings of the 60 GHz oxygen complex, which are only a few degrees Celsius and stable, and the receiver sensitivities of ~0.1 K for 16 s integration, which are negligibly small in comparison to typical signal variations of tens of degrees.

Water vapor higher in the troposphere is at lower pressure and hence exhibits a narrower line width. Thus a given amount of water vapor at high altitudes absorbs and emits more strongly at the line center than does the same amount at lower altitude. This altitude dependence of water vapor emission can be expressed approximately as

$$T_B(\nu) \approx T_{Bs}(\nu) + \int_0^\infty \rho_{H_2O}(h) W_v(\nu,h) dh, \qquad (1)$$

where $T_{Bs}(\nu)$ is the brightness temperature contribution of the sea and atmospheric oxygen alone, and $W_v(\nu,h)$ is the water vapor weighting function at frequency ν and height h (m); Eq. (1) defines $W_v(\nu,h)$. This weighting function definition differs from those generally used at infrared wavelengths because it is useful to explicitly include the contributions of the radiation reflected from the ocean surface; the reflected component usually represents about one-third of the total signal at these wavelengths.

Water vapor weighting functions for channels 1 and 2, i.e. 22.235 and 31.4 GHz, are presented in Fig. 2. The frequency 22.295 GHz was used in Fig. 2 for channel 1 because it is the center of one i.f. passband, and quite representative. The 22.295 GHz weighting function increases very slowly with altitude from its value at the surface, whereas at 31.4 GHz the weighting function decreases with altitude.

The abundance of water vapor in the atmosphere is estimated by computing a linear combination of the channel 1 and 2 brightness temperatures T_{B_1} and T_{B_2},

$$V = -4.03 + 0.0841 T_{B_1} - 0.0515 T_{B_2}. \qquad (2)$$

The expression for the water vapor estimate V (g cm^{-2}) given in (2) was obtained by a multi-dimensional regression analysis based upon theoretical T_B's computed for ~150 radiosondes at 12 latitudes between 7° and 75°N over a two-year period. The method is essentially that described by Rosenkranz *et al.* (1972). These atmospheres were presumed to be cloud-free. The expression has been altered slightly to compensate for instrument calibration errors. Small corrections on the order of 0.1 g cm^{-2} were made for variations in the ocean surface temperature. The climatic average sea surface temperature was assumed; errors of several degrees are not significant. The emissivity $\bar{E}$ was determined as a function of temperature and frequency from the equations given by Stogryn (1971). These equations were based on laboratory measurements by Saxton and Lane (1952), Grant et al. (1957), and others.

The absorption by water clouds was assumed to be

$$\alpha_{CLD} = 3.95 \rho_L \nu^2 10^{-(6+0.0122T)} \text{ [cm}^{-1}\text{]}, \qquad (3)$$

where ρ_L is cloud density (g m^{-3}). This formula was inferred by Staelin (1966) from data presented by Goldstein (1951), and is accurate within several percent when the cloud drop diameters are small compared to $\lambda/50$, i.e., smaller than ~100 μ. This is true for most non-raining clouds, and thus the microwave absorption is directly proportional to the integrated liquid water abundance with more precision than is obtainable from most other cloud sensing techniques.

The liquid water estimates are constructed in such a way that the presence of water vapor does not cause excessive spurious inference of liquid water. The equation used to estimate atmospheric liquid water abundances L (g cm^{-2}) over ocean is

$$L = -0.404 - 1.54 \times 10^{-3} T_{B_1} + 4.09 \times 10^{-3} T_{B_2}, \qquad (4)$$

where the coefficients are those determined by Rosen-

kranz *et al.* (1972) using regression techniques based on theoretical microwave emission spectra computed for 334 National Weather Service (NWS) radiosondes from arctic, tropical, and midlatitude stations.

The sensitivity of the liquid water estimates L to the altitude distribution of water vapor can be expressed in terms of $W_L(h)$, which is defined so that

$$L \approx L_0 + \int_0^\infty \rho_v(h) W_L(h) dh. \quad (5)$$

The estimate L exceeds the true value L_0 by an amount proportional to the water vapor distribution $\rho_v(h)$ (g cm^{-3}) weighted by $W_L(h)$, where h is altitude (cm). The value of $W_L(h)$ may be found from Eqs. (1), (4) and (5) and is presented in Fig. 2. It indicates that the liquid water estimate can vary by $\sim$0.01 g cm^{-2} for reasonable variations in water vapor altitude distribution, underestimates arising when the water vapor is high in the atmosphere, and overestimates when it is near the surface.

3. Accuracy of NEMS measurements

The accuracies of NEMS measurements were determined both theoretically and empirically. Theoretical accuracies were determined by inferring water vapor and liquid water densities from brightness temperatures computed theoretically for realistic ensembles of model atmospheres, as discussed by Rosenkranz *et al.* (1972).

The dominant source of error in the water vapor estimates was variations in the altitude distribution of water vapor. The sensitivity of V estimates to the altitude distribution of water vapor can be found by computing, using (2), the appropriate linear combination of the channel 1 and 2 water vapor weighting functions that were defined in (1). That is, the water vapor estimate can be expressed as

$$V \approx V_0 + \int_0^\infty \rho_V(h) W_v(h) dh, \quad (6)$$

where V_0 is a small constant and W_v is proportional to $0.0841\,W_1 - 0.0515\,W_2$ [see Eq. (2)]. Eq. (6) defines the retrieval weighting function, which is different from the single-frequency weighting function defined in (1). This retrieval weighting function W_v is plotted in Fig. 2 and clarifies how errors can be introduced by variations in the altitude distribution of water vapor. The figure shows that the NEMS estimates are approximately twice as sensitive to vapor in the upper troposphere as they are to vapor at sea level. Fortunately the atmospheric water vapor distribution is generally concentrated close to earth and decays approximately exponentially with a scale height of $\sim$2.2 km; it is sufficiently stable that total rms errors of $\lesssim$0.1–0.2 g cm^{-2} are incurred, depending on climate. Greater accuracies could be obtained with additional frequencies of observation so that one could synthesize a water vapor retrieval weighting function $W_v(h)$ that is more nearly independent of altitude.

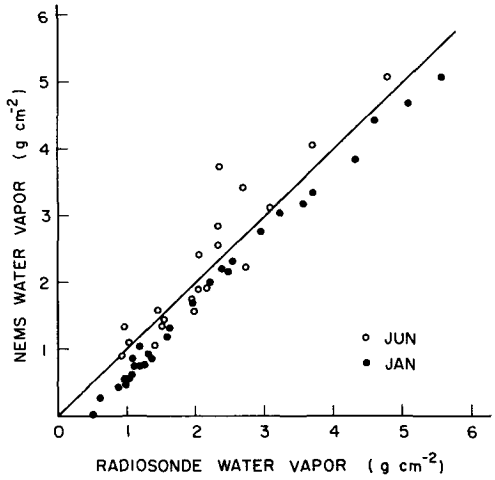

FIG. 3. Comparison of water vapor abundances derived from NEMS and from nearby radiosondes for January and June, 1973.

A second source of error is that the inversion algorithm used is linear in brightness temperature T_B whereas T_{B_1} saturates near 280 K for $M_V \gtrsim 10$ g cm^{-2}. This source of error is greatest in the tropics. Although it could be corrected, it is generally smaller or comparable to other sources of error, and is not corrected here. There is some tendency for these errors to cancel the errors introduced by variations in the scale height of the water vapor distribution. That is, regions of ascending air, as in the extremely humid ITCZ, naturally tend to have larger scale heights than regions of descending air.

The accuracy of NEMS water vapor estimates was tested empirically by comparison with standard radiosondes launched from ships or islands. Comparisons were made only if the radiosonde and NEMS were separated less than 200 km. For latitudes outside the equatorial belt ($\pm$30°) the separations were less than 2.5 h, and inside the belt the separations were less than 4.5 h. The soundings were made at scattered longitudes and latitudes, although $\sim$85% of the soundings were made in the Northern Hemisphere.

The first data set contains 31 radiosonde records for January 1973, and the second set contains 21 for June 1973. The comparison between the NEMS-derived water vapor and the corresponding radiosondes is presented in Fig. 3. The mean error for the January data is 0.35 g cm^{-2} and the rms error about the mean is 0.12 g cm^{-2}. For June the corresponding numbers are $-$0.09 and 0.44, the increase in rms errors in June most likely being due to a greater predominance of small scale structure during the summer season. Comparable discrepancies were obtained between Cosmos-243 and radiosondes by Basharinov *et al.* (1969) and Gurvich and Demin (1970).

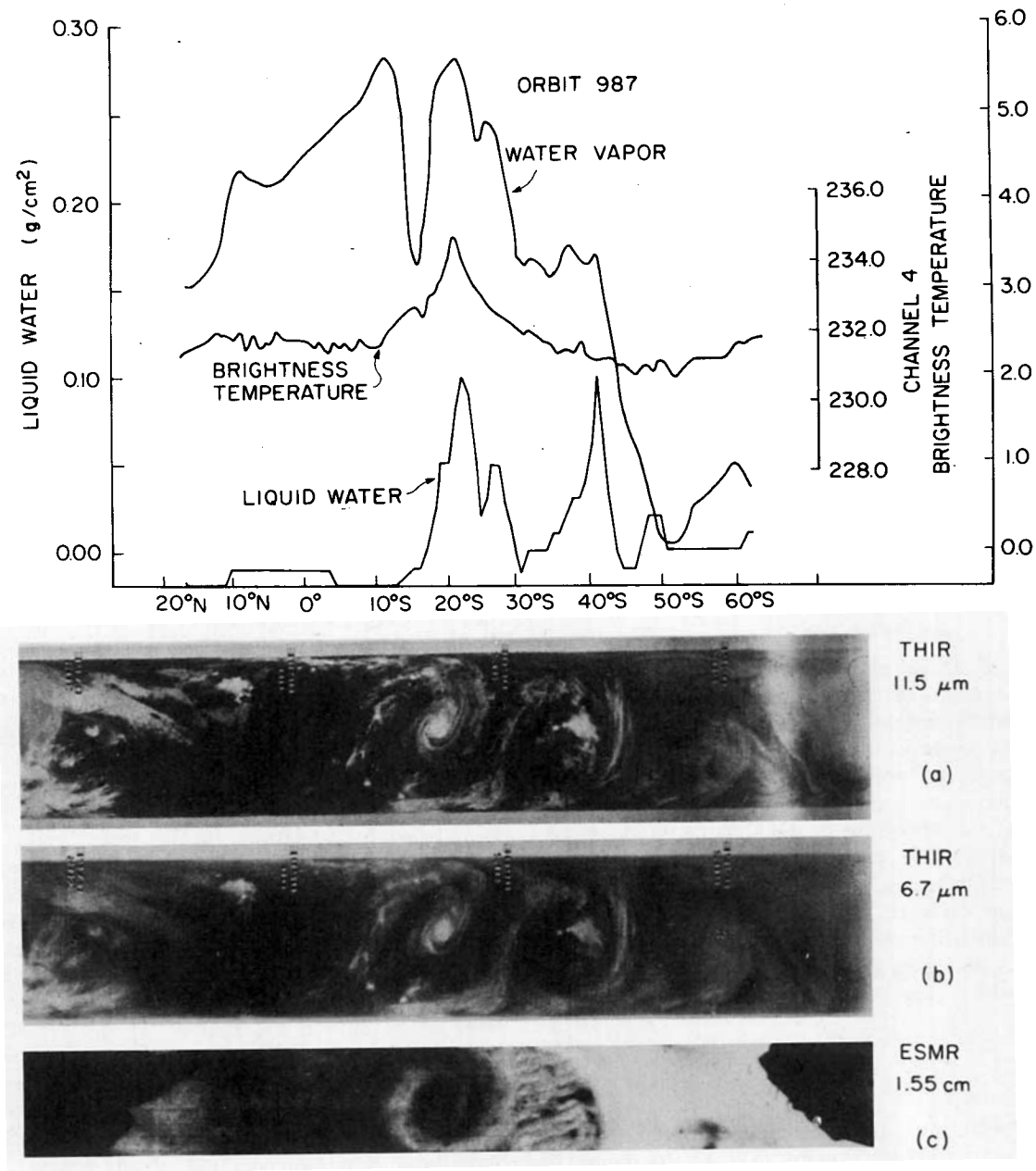

FIG. 4. Tropical cyclone viewed at night by NEMS, THIR and ESMR on 22 February 1973 south of India near 62°E longitude.

The origin of the fairly large mean error in January is unknown, but it could arise from 1) errors in T_B calibration of ~5 K, 2) theoretical expressions for ocean surface emissivity which are too large by ~0.04, or 3) errors arising from statistical differences between the a priori December data set and the actual January data. The most likely explanation is perhaps that calibration errors are largely responsible, but further study would be necessary to test this hypothesis.

The principal source of error for thin clouds is introduced by variations of the ocean surface and of the altitude distribution of water vapor, as discussed earlier. Rosenkranz *et al.* (1972) estimated that altitude variations of water vapor alone would contribute ~0.006 g cm^{-2} rms error; this was based on 334 radiosondes launched in summer at various latitudes. For somewhat heavier clouds the errors arise increasingly from the temperature dependence of the absorption coefficient. If the assumed average cloud temperature is in error by 10 K, this introduces an error of ~30% in the liquid water estimate.

In rain cells two other sources of error also arise. First, the drop sizes are no longer negligibly small, but can exceed 1 mm. As the nominal drop size increases, the absorption may first increase by a factor of ~4 above the values given in Eq. (3), and then fall back below them. This is due to the resonant absorption and scattering effects that arise as the wavelength of radiation within the droplets approaches twice the drop diameter, an effect first considered by Mie (1908) and reviewed by Stratton (1941) and others.

The second source of error arises because cells that rain more than ~5 mm h^{-1} become sufficiently opaque that the liquid water content cannot be fully sensed. In that case NEMS is responsive more nearly to the areal extent of the opaque cells rather than to their actual water content. In particular, the liquid water content of the intertropical convergence zone (ITCZ) and similar major precipitation zones is probably underestimated.

Careful solar observations at 16 and 30 GHz by Hogg (1973) in New Jersey have shown that the typical size for rain cells precipitating 5 mm h^{-1} is 11

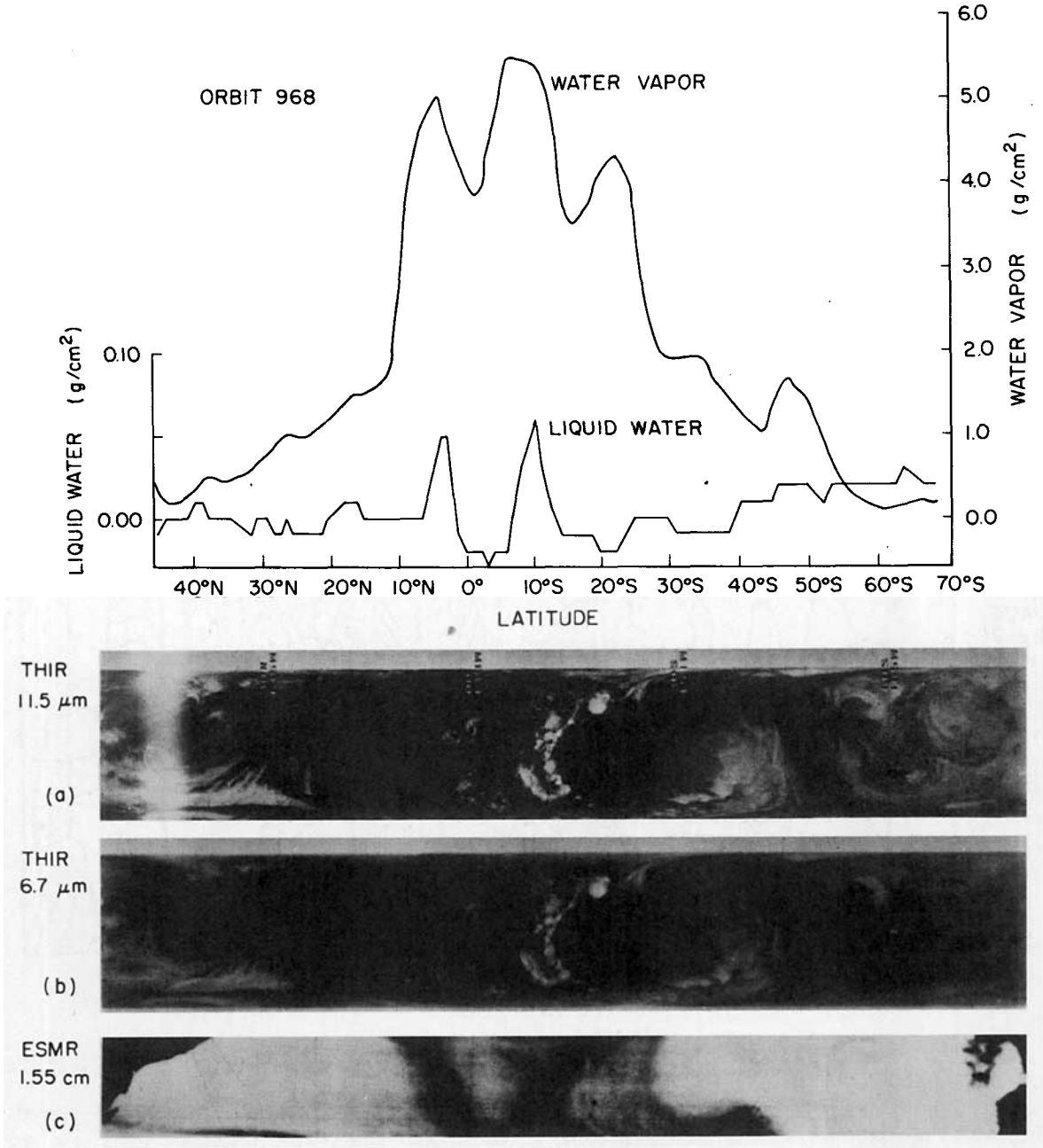

FIG. 5. Intertropical convergence zone viewed at night by NEMS, THIR and ESMR on 21 February 1973 in the central Pacific near 145°W longitude.

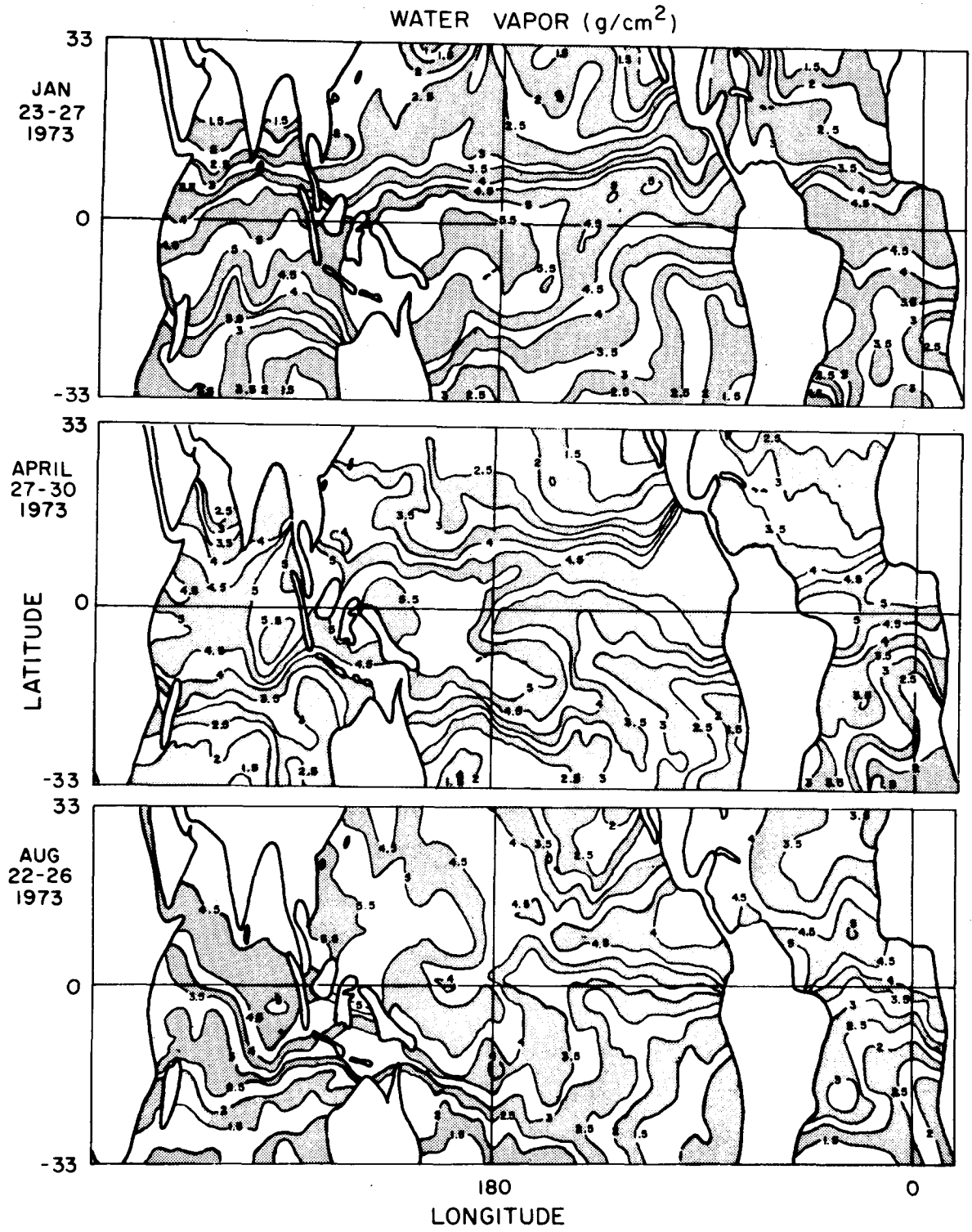

FIG. 6. Average water vapor (g cm^{-2}) observed by NEMS for the periods 22–27 January, 27–30 April and 22–26 August, 1973. The continents are outlined and free of contours.

km, and that this dimension decreases to 2 km for 100 mm h^{-1}. Radar observations, such as those of Freeman (1976), yield similar results. These data suggest that most single opaque precipitation cells would occupy less than 0.3% of the instantaneous field viewed by NEMS and only large clusters of such cells would introduce significant errors.

It is very difficult to determine experimentally the

accuracy of the NEMS liquid water estimates because there are no reliable sources of comparison data. Aircraft, radiosondes, or other *in situ* sensors are not able to sample enough of the region viewed by the spacecraft, and weather radar is too sensitive to the drop size distribution. The most reliable accuracy estimates for NEMS are therefore deduced either theoretically for an appropriate ensemble of model atmospheres, as discussed by Rosenkranz *et al.* (1972), or experimentally by consideration of liquid water retrievals in cloud-free regions, as discussed below. These approaches both suggest the rms accuracy is approximately 0.01 g cm^{-2} in the absence of strong sea-state effects.

4. Observations of storms and fronts

The uniqueness of the NEMS observations of atmospheric water lies in the 1) cloud penetration ability, 2) quantitative estimates of total liquid water, and 3) quantitative estimates of total precipitable water vapor that are more responsive to humidity variations in the bottom 1–2 km than are most other remote sensors. Such microwave data provide a novel view of the structure of storms and fronts that cannot readily be obtained in any other way.

In Fig. 4 is presented a nighttime view of a large tropical cyclone located between India and Antarctica on 22 February 1973. The morphology of the storm is best shown in the infrared and microwave images. Similar images have been discussed by Allison *et al.* (1974). The 11.5 μm THIR (*T*emperature *H*umidity *I*nfrared *R*adiometer) image shows the general cloud patterns, with white patches corresponding to colder clouds. The darker portions of the 6.7 μm image indicate regions of dryer air in the upper troposphere. The 6.7 μm band is dominated by water vapor absorption, and dryer air permits the hotter lower altitude regions to be sensed, yielding the dark regions in the figure.

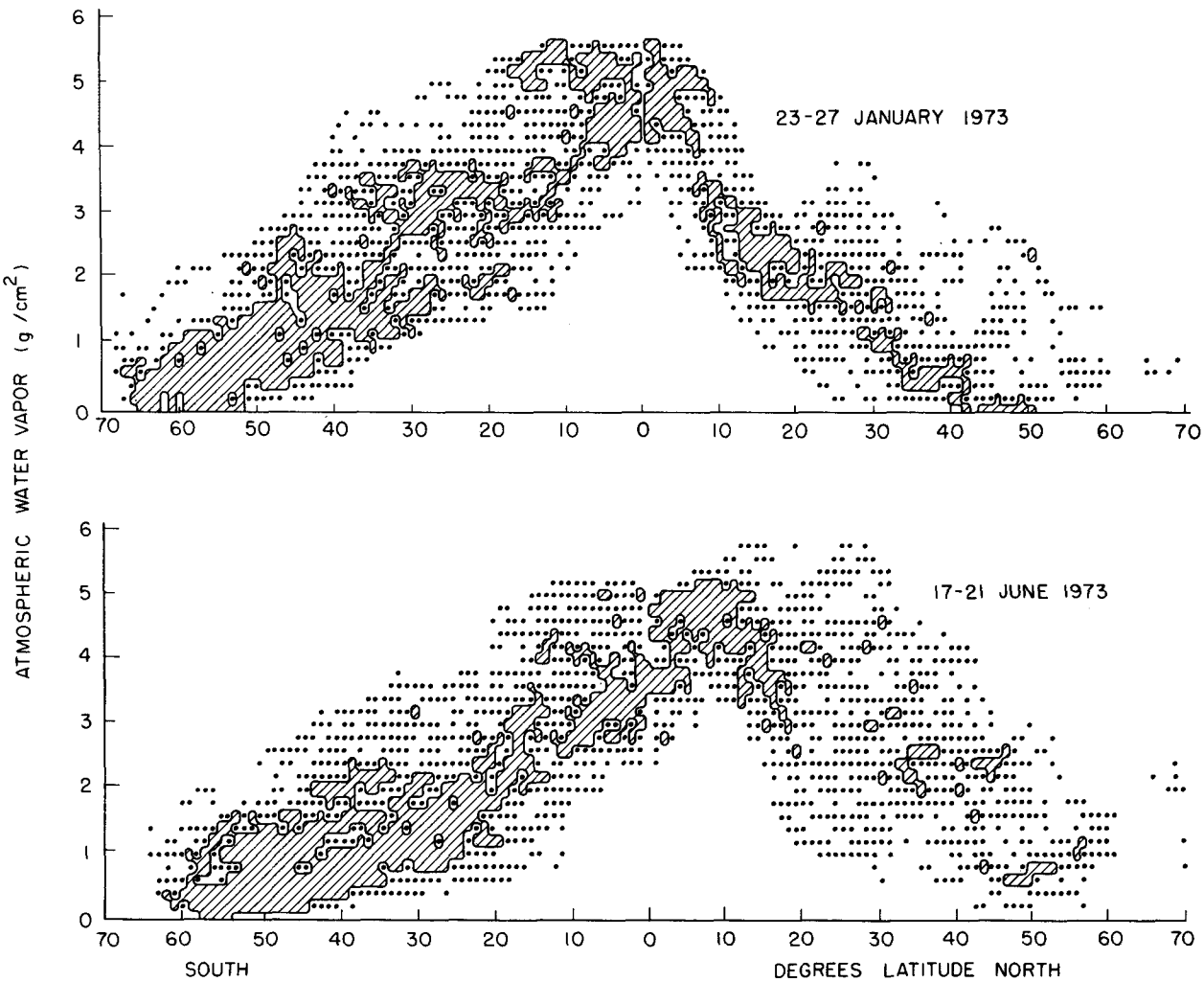

FIG. 7. Number of NEMS observations of each humidity value (g cm^{-2}) at each latitude over ocean, unnormalized for the number of such soundings at each latitude. Dots signify one or two occurrences, and cross hatching signifies more than two.

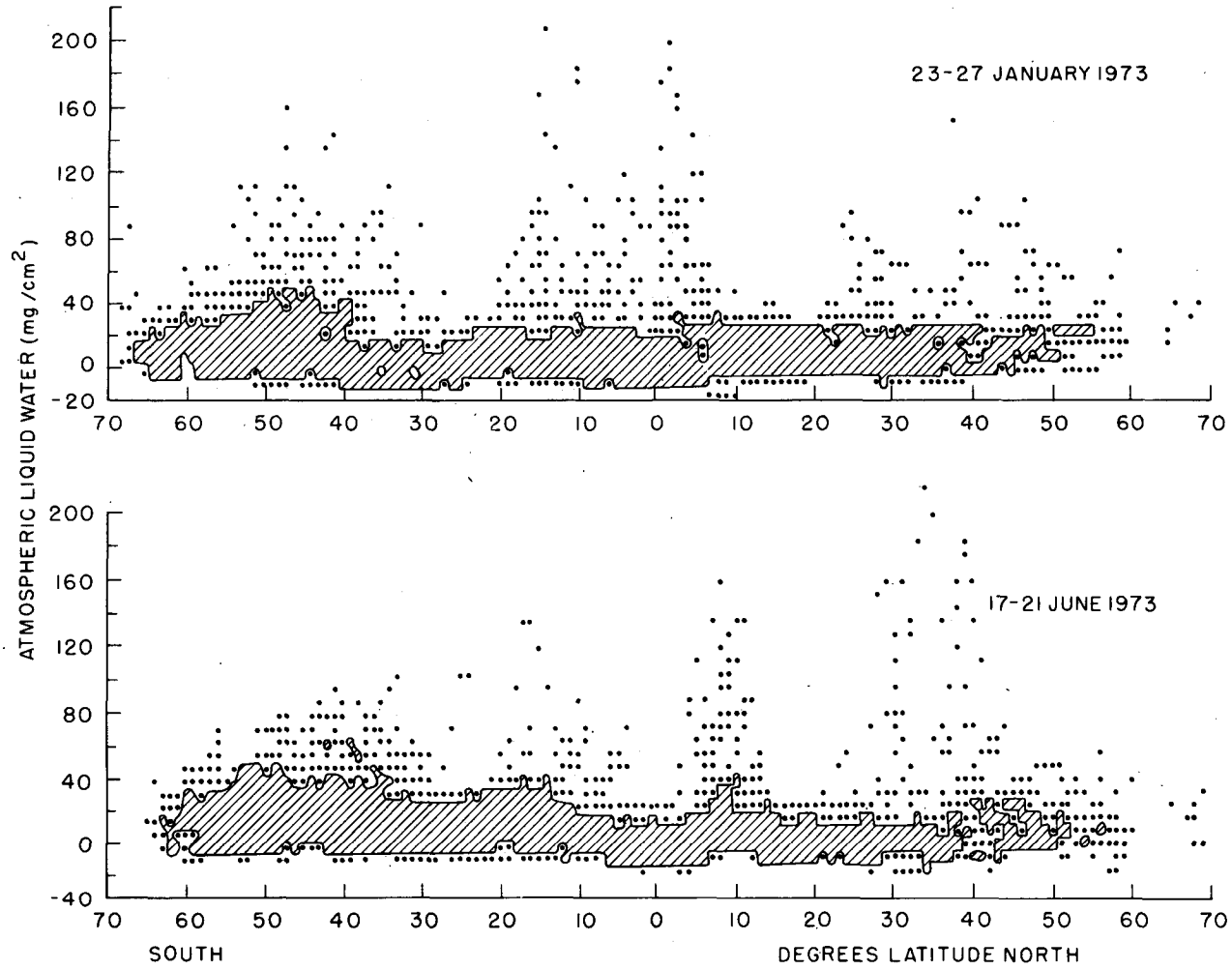

FIG. 8. Number of NEMS observations of each value of liquid water (g cm^{-2}) over ocean, unnormalized for the number of such soundings at each latitude. Dots signify one or two occurrences, and cross hatching signifies more than two.

The ESMR (*E*lectrically *S*canned *M*icrowave *R*adiometer) image responds to the integrated humidity by virtue of the water vapor thermal emission as seen against the cold background of the ocean. The ESMR instrument has been discussed by Wilheit (1972). This cold background, a result of the low microwave emissivity of sea water, together with the much greater atmospheric opacity at 6.7 μm, are largely the reasons why the microwave and 6.7 μm infrared data differ so markedly. Infrared images at any wavelength are less sensitive to humidity variations in the bottom kilometer of the atmosphere than are these microwave wavelengths because the kinetic temperature of the water vapor there is much more nearly the same as the infrared emission temperature of the ocean, thus diminishing the contrast, and because the bottom kilometer is often overlaid at many infrared wavelengths, including 6.7 μm, by nearly opaque atmospheric layers at higher altitudes.

The NEMS estimates of water vapor and liquid water show plainly that three major air masses are involved in this tropical cyclone; i.e. the tropical air mass with precipitable water near 5 g cm^{-2}, an air mass near 3.2 g cm^{-2}, and polar air below 1 g cm^{-2}. The liquid water is located near the eye and in the band near 27°S. Strong precipitation is also evident near 41°S.

The nature of the storm is also indicated by the channel 4 54.9 GHz brightness temperature, which corresponds to the average air temperature at 11±4 km altitude. The observed warm core of the storm is geostrophically consistent with typical azimuthal wind velocities diminishing at higher altitudes. Warm cores aloft have been observed, for example, in Hurricane Hilda by Hawkins and Rubsam (1968), but few observations extend over such large geographic regions as are presented here.

Another nighttime equatorial pass, this time over the Pacific Ocean, is presented in Fig. 5 for 21 February 1973. The intertropical convergence zone (ITCZ) is plainly evident, as is the sharp contrast between the humid air mass (3.3–5.5 g cm^{-2}) and the dry air (0–2.0 g cm^{-2}). The relatively more humid band near

50°S, evident in the NEMS data, appears as a dry band in the 6.7 μm infrared water vapor data, again illustrating the different altitude responses of the two systems.

The liquid water estimate for the large equatorial precipitation cells, 0.05 g cm^{-2}, is low because the antenna does not resolve the single cells but rather averages over adjacent non-precipitating regions as well. The increase in inferred liquid water content south of 40°S is probably not due to clouds but rather to heavy seas and to water temperatures below those assumed in derivation of the inversion algorithm. The corrections for climatological sea surface temperature made in preparation of Fig. 3 were not made for the data presented in Figs. 4 and 5.

5. Global observations of water vapor and liquid water

Using the procedures described earlier, the water vapor distribution over ocean was determined for 4-day periods in winter, spring and summer, 1973. The average water vapor concentrations are shown in Fig. 6 for the periods 23–27 January, 27–30 April and 22–26 August, 1973. The figures are expanded in latitude to clarify the complicated humidity patterns near the equator.

In January the sharp gradient in humidity between 5° and 15°N is particularly prominent. The effects of the trade winds can also be seen in all three seasons. The northern clockwise and southern counterclockwise rotations are evident, particularly in April and August. A similar map of the eastern Pacific has been presented by Wark (1974) for 10 September 1973. It was based on clear-air 19 μm water vapor data from the VTPR infrared sounder on the NOAA-2 satellite.

Statistical distributions of observed humidity over ocean are presented in Fig. 7 for 23–27 January and 17–21 June, 1973. Blanks indicate no events, dots indicate 1 or 2 events, and cross hatching indicates more than 2 events. The asymmetry between the northern and southern hemispheres evident in Fig. 6 is also evident here. In the Northern Hemisphere it can be seen that the winter humidity distribution is much less variable than the summer distribution, as noted earlier in the discussion of Fig. 3. The statistics are slightly distorted because NEMS views ocean in the Southern Hemisphere more than in the north.

Similar histograms of the inferred liquid water distribution are presented in Fig. 8 for the same periods in January and June. The inferred liquid water and water vapor abundances in Figs. 7 and 8 were corrected for the seasonal variations in sea surface temperature, independent of longitude. The corrections near the poles are ~0.03 g cm^{-2} greater than at the equator, for both liquid water and water vapor estimates.

The accuracy of the liquid water determinations can be estimated from the scatter of those determinations which are near 0.0 g cm^{-2}. This is so because over half the time the liquid water content of the atmosphere is essentially zero. The rms scatter of the dryest half of the estimates and therefore the accuracy of the NEMS liquid water determinations is estimated to be approximately 0.01 g cm^{-2}, with the dominant sources of error being sea surface effects and variations in water vapor distribution in altitude.

The large number of soundings below 30°S yielding 0.03–0.04 g cm^{-2} liquid water probably includes many that are dominated by sea state effects associated with strong westerly winds. As discussed by Rosenkranz and Staelin (1972), winds near 25 mph would yield erroneous liquid water determinations near 0.03 g cm^{-2}, consistent with values inferred for the southern oceans. Sea state effects and atmospheric liquid water abundances are very difficult for NEMS to distinguish because they have similar spectra.

6. Conclusions and future potential

The NEMS experiment has demonstrated the ability of a two-channel microwave spectrometer to determine integrated abundances of water vapor and liquid water with estimated rms accuracies of 0.2 and 0.01 g cm^{-2}, respectively. Determination of these accuracies is difficult because of the lack of accurate data for comparison. The ultimate capability of passive microwave spectrometers to sound atmospheric water vapor and liquid water from space is not now known, but it certainly exceeds the encouraging initial results presented here. Additional frequencies near 1 cm wavelength would reduce the errors introduced by variable water vapor scale heights, and frequencies ranging from 0.3–20 cm and observed with dual polarization at an oblique angle would reduce errors introduced by uncertainties in sea temperature and sea state. Such spectrometers may also yield information about water vapor scale heights (Staelin, 1966) and about liquid water over land (Staelin *et al.*, 1975).

The data, particularly when combined with high resolution images such as those from ESMR and THIR, provide a unique portrait of oceanic weather systems. These portraits can be considerably improved, for microwave spectrometers capable of global mapping with 3 km resolution appear quite feasible.

Acknowledgments. We appreciate discussions with T. T. Wilheit concerning ESMR, and the assistance received from the NASA Goddard Space Flight Center, where the THIR and ESMR images were processed. Environmental Research and Technology, Inc., kindly provided the radiosonde data used for the regression analyses. NEMS was fabricated under the direction of F. T. Barath and E. J. Johnston and benefited from the participation of A. H. Barrett, N. E. Gaut, W. B. Lenoir, W. Nordberg, and P. W. Rosenkranz. The work was supported by NASA Contracts NAS 7-100 and NAS 5-21980.

REFERENCES

Akvilonova, A. G., A. E. Basharinov, A. K. Gorodetskii, A. S. Gurvich, M. S. Krilova, B. G. Kutuza, D. T. Matveev and A. P. Orlov, 1973: Determination of meteorological parameters with measurements from the satellite Cosmos-384. *Atmos. Oceanic Phys.*, **9**, 187–189.

Allison, L. J., E. R. Rodgers, T. T. Wilheit and R. W. Fett, 1974: Tropical cyclone rainfall as measured by the Nimbus-5 electrically scanning microwave radiometer. *Bull. Amer. Meteor. Soc.*, **55**, 1074–1089.

Barath, F. T., A. H. Barrett, J. Copeland, D. E. Jones, and A. E. Lilley, 1964: Mariner 2 microwave radiometer experiments and results. *Astron. J.*, **69**, 49–58.

Barrett, A. H., and V. K. Chung, 1962: A method for the determination of high-altitude water-vapor abundance from ground-based microwave observations. *J. Geophys. Res.*, **67**, 4259–4266.

Basharinov, A. E., A. S. Gurvich and S. T. Yegorov, 1969: Determination of geophysical parameters from radio measurements from Cosmos-243. *Dokl. Akad. Nauk SSSR*, **188**, 1273–1276.

Freeman, L. E., 1976: Sizes and intensities of mesoscale precipitation areas as depicted by digital radio data. S.M. thesis, Dept. of Meteorology, MIT.

Goldstein, H., 1951: Attenuation by condensed water. *Propagation of Short Radio Waves*, D. E. Kerr, Ed., McGraw-Hill, 671–692.

Grant, E. H., T. J. Buchanan, and H. F. Cook, 1957: Dielectric behavior of water at microwave frequencies. *J. Chem. Phys.*, **26**, 156–161.

Grody, N. C., 1976: Remote sensing of atmospheric water content from satellites using microwave radiometry. *IEEE Trans. Antennas Propag.*, **AP-24**, 155–162.

Gurvich, A. S., and V. V. Demin, 1970: Total atmospheric humidity measured by the Cosmos-243 satellite. *Atmos. Oceanic Phys.*, **6**, 771–779.

Hawkins, Harry F., and D. J. Rubsam, 1968: Hurricane Hilda, 1964, II: Structure and budgets of the hurricane on October 1, 1964. *Mon. Wea. Rev.*, **96**, 617–636.

Hogg, D. C., 1973: Intensity and extent of rain on earth-space paths. *Nature*, **243**, 337–338.

Mie, G., 1908: *Ann. Phys.*, **25**, 377–445.

Rosenkranz, P. W., and D. H. Staelin, 1972: Microwave emissivity of ocean foam and its effect on nadiral radiometric measurements. *J. Geophys. Res.*, **77**, 6528–6538.

——, F. T. Barath, J. C. Blinn III, E. J. Johnston, W. B. Lenoir, D. H. Staelin and J. W. Waters, 1972: Microwave radiometric measurements of atmospheric temperature and water from an aircraft. *J. Geophys. Res.*, **77**, 5833–5844.

Saxton, J. A., and J. A. Lane, 1952: Electrical properties of sea water. *Wireless Engineer*, **29**, 269–275.

Staelin, D. H., 1966: Measurements and interpretation of the microwave spectrum of the terrestrial atmosphere near 1-centimeter wavelength. *J. Geophys. Res.*, **71**, 2875–2881.

——, A. H. Barrett, J. W. Waters, F. T. Barath, E. J. Johnston, P. W. Rosenkranz, N. E. Gaut and W. B. Lenoir, 1973: Microwave spectrometer on the Nimbus-5 satellite: meteorological and geophysical data. *Science*, **182**, 1339–1341.

——, A. L. Cassel, K. F. Kunzi, R. L. Pettyjohn, R. K. L. Poon, P. W. Rosenkranz and J. W. Waters, 1975: Microwave atmospheric temperature sounding: effects of clouds on the Nimbus-5 satellite data. *J. Atmos. Sci.*, **32**, 1970–1976.

Stogryn, A., 1971: Equations for calculating the dielectric constant of saline water. *IEEE Trans. Microwave Theory Tech.*, **MTT-19**, 733–736.

Stratton, J. A., 1941: *Electromagnetic Theory*. McGraw-Hill, 615 pp.

Toong, H. D., and D. H. Staelin, 1970: Passive microwave spectrum measurements of atmospheric water vapor and clouds. *J. Atmos. Sci.*, **27**, 781–784.

Wark, D. Q., 1974: Meso-scale variations in atmospheric water vapor in tropical regions deduced from VTPR measurements. *Proc. IUGG*, IAMAP, Melbourne, 315–320.

Waters, J. W., K. F. Kunzi, R. L. Pettyjohn, R. K. L. Poon and D. H. Staelin, 1975: Remote sensing of atmospheric temperature profiles with the Nimbus-5 microwave spectrometer. *J. Atmos. Sci.*, **32**, 1953–1969.

Wilheit, T. T., 1972: The electrically scanning microwave radiometer (ESMR) experiment. *Nimbus-5 Users Guide*, NASA Goddard Space Flight Center, 55–105.